

*Invited article for PEDOSPHERE***Running Title: CADMIUM SORPTION MECHANISMS ON SOIL MINERAL SURFACES****A review of cadmium sorption mechanisms on soil mineral surfaces revealed
from synchrotron-based X-ray absorption fine structure spectroscopy:
Implications for soil remediation**Xinxin MO¹, Matthew G. SIEBECKER², Wenxian GOU¹, Ling LI³, Wei LI^{1,*}¹*Key Laboratory of Surficial Geochemistry, Ministry of Education, School of Earth Sciences and Engineering, Nanjing University, Nanjing 210023 (China)*²*Department of Plant and Soil Science, Texas Tech University, Lubbock, Texas 79409 (USA)*³*State Key Laboratory of Environmental Geochemistry, Institute of Geochemistry, Chinese Academy of Sciences, Guiyang 550081 (China)***ABSTRACT**

Sorption of cadmium (Cd) is one of its most important chemical processes in soils, which affects its fate and mobility in soils and waters and eventually controls its bioavailability. In order to fundamentally understand the Cd sorption/desorption phenomenon in soil systems, X-ray absorption fine structure (XAFS) spectroscopy has been applied in numerous studies to provide molecular-level information which characterizes the surface adsorption and precipitation reactions that Cd can undergo. This information greatly improves our current knowledge of the soil chemical reactions of Cd. This paper critically reviews the mechanisms of Cd sorption/desorption at the mineral/water interface based on XAFS studies performed in the past twenty years. An introduction to basic concepts for describing sorption processes is provided, followed by a detailed interpretation of XAFS

*Corresponding author. Email: liwei_isg@nju.edu.cn

theory and experimental data collection and processing, and finally a discussion of atomic/molecular scale Cd sorption mechanisms at soil mineral/water interfaces is provided. Particular emphasis is paid to the literature discussing Cd adsorption and speciation to iron, manganese and aluminum oxides, as well as aluminosilicate minerals. Multiple sorption mechanisms of Cd on these minerals were found, spanning from outer-sphere, to inner-sphere, to precipitation which depend on mineral type, surface loading and pH. In addition, we also discussed the application of complementary techniques (e.g., ^{113}Cd NMR and molecular simulations) in probing Cd sorption mechanisms. A summary of these literature will shed light on the strategy for environmental remediation of Cd-contaminated soil.

Key Words: cadmium sorption, soil mineral surfaces, soil remediation, synchrotron-based X-ray fine structure spectroscopy,

1. INTRODUCTION

Cadmium (Cd) is the second element of IIB group, which has been recognized to be a toxic, carcinogenic and teratogenic heavy metal (U.S. Department of Health and Human Services, 2012). Cd is classed as a human carcinogen (group 1) by the International Agency for Research on Cancer of the World Health Organization (WHO). The predominant pathway of Cd exposure to humans is through the diet, especially rice consumption (Järup and Åkesson, 2009; Satarug *et al.*, 2010; Chaney, 2012). The world's first documented incidence of mass poisoning by Cd-polluted rice, itai-itai disease occurring in Japan in the 1950s, caused about 300 people to have osteomalacia and marked decalcification (Nogawa and Kido, 1993). China is a major rice production and consumption country and suffers from Cd-contamination in rice. The background level of Cd in soils in China ranges from 0.01~1.80 mg kg⁻¹ with an average of 0.163 mg kg⁻¹, slightly less than that worldwide, which ranges from 0.01~2.0 mg kg⁻¹ with an average of 0.35 mg kg⁻¹. While the soil quality standard, i.e., the maximum allowable concentration of Cd contaminants in soils, is specified as 0.3~0.6 mg kg⁻¹ in China, whereas that worldwide almost varies from 0.8 mg kg⁻¹ to 5.0 mg kg⁻¹ (Zhao *et al.*, 2014). Once the Cd content in soils exceed the standard value, it means some timely control and treatments could be required. According to the *Report on the national general survey of soil* by the Ministry of Environmental Protection and Ministry of Land and Resources of China (2014), Cd is at the top of

the list of inorganic contaminants, and exceeds the safety standard by a rate of 7.0%. Additionally, there also occur plenty of regional excessive levels and pollution incidents of Cd around the world, for example, in Hunan Province, China.

Anthropogenic activities were the major input of Cd to agriculture soils, which include metal mining and smelting, sewage irrigation, and fertilizer application (Hu and Cheng, 2013; Wen *et al.*, 2015; Luo *et al.*, 2009). In addition to anthropogenic activities, natural weathering of Cd-rich sedimentary rock can also lead to elevated Cd levels in soils. The concentration of natural-occurring Cd in the arable soils influenced by parent rocks of black rock series in the Three Gorges Region of southwestern China is up to 42 mg kg⁻¹ (Liu *et al.*, 2015), which is around 80 times the value of the surface soils (0.53 mg kg⁻¹) (Kabata-Pendias and Pendias, 2001).

In soils, the negative impact of Cd is determined by its bioavailability, which characterizes the degree of total Cd that can be taken up by biota. There are many empirical methods to evaluate soil Cd bioavailability, which include *in situ* diffusive gradients in thin film (DGT) and *ex situ* single step extraction methods (Wang *et al.*, 2017; Smilde *et al.*, 1992; Krishnamurti *et al.*, 1995). However, in principle, cadmium bioavailability is controlled by soil chemical reactions (Chen *et al.*, 2000; Krishnamurti *et al.*, 1995) at soil mineral/water interfaces, including adsorption/desorption, precipitation/dissolution, and Cd–ligand complex formation (Bolan *et al.* 2013).

Because of the importance of soil mineral/water interface reactions, a mechanistic understanding of the sorption reactions of Cd is fundamentally important for risk assessment and soil remediation. In the past thirty years, X-ray absorption fine structure spectroscopy (XAFS) has been widely applied to elucidate metal sorption mechanisms at the molecular level (Hayes *et al.*, 1987; Chisholm-Brause *et al.*, 1990; Scheidegger *et al.*, 1996; Gräfe *et al.*, 2007; Li *et al.*, 2011). XAFS is an element-specific technique that yields molecular- and atomic-level structural information on interatomic distances, and number and type of atomic coordination (Kelly *et al.*, 2008). Based on these structural parameters, the mechanism of outer-sphere complexation, inner-sphere surface complexation, and surface precipitation can be distinguished. In this review, we provide an introduction of the basic concepts of metal sorption phenomena on soil minerals, followed by a detailed description of EXAFS data collection and data processing, and finally a thorough review XAFS studies on the sorption mechanisms of Cd at soil mineral surfaces.

Furthermore, future perspectives on the application of new methods (e.g., ^{113}Cd nuclear magnetic resonance (NMR) (Di Leo and O'Brien, 1999) in probing Cd interface chemistry are discussed.

2. GENERAL CONCEPTS OF SORPTION REACTIONS IN SOIL CHEMICAL PROCESSES

Bioavailability of contaminants in soils and sediments is affected by a series of individual physical, chemical, and biological interactions that determine the exposure of plants and animals to chemicals (NRC 2003), which is shown schematically in Fig. 1. The bioavailability processes include: (i) contaminant interactions between phases, as a result of which contaminants reside in a bound state (associated with soil or sediment particles) or a released state (dissolved in a liquid or gas phase); (ii) transport of contaminants (both the bound and released form) to organism; and (iii) passage across physiological membrane. With respect to the process of contaminant–solid interactions, i.e., process (i), sorption reactions at the mineral/water interface is of great significance to control the speciation, mobility, fate, and bioavailability of contaminants in soil environments.

Fig. 1 Schematic diagram of bioavailability processes from the National Research Council (2003): (A) Contaminant interactions between phases, (B) Transport of bond contaminants to organism, (C) Transport of released contaminants to organism, (D) Passage across physiological membrane, and (E) circulation within organism, accumulation in target organ, toxicokinetics, and toxic effects, reprinted with permission from *Bioavailability of Contaminants in Soils and Sediments*, Copyright (2003) by The National Academies of Sciences, Courtesy of the National Academies Press, Washington, D.C. Possible sorption mechanisms at the mineral-water interface: (I) Outer-sphere surface complexes, (II) Inner-sphere surface complexes, (III) Surface precipitation, and (IV) Substitution (or surface incorporation).

Sorption can be defined as the phenomenon where aqueous ions, complexes or molecules accumulate at the interface of a solid substance and the aqueous solution. In general, there are four main mechanisms of sorption (Fig. 1) : (i) outer-sphere and (ii) inner-sphere surface complexation can be collectively referred to as adsorption, that is, soluble species aggregate on the surface of minerals without forming a three-dimensional molecular arrangement, among which

inner-sphere complexes are generally more strongly bound to surfaces than outer-sphere complexes; (iii) surface precipitation or polymerization, which forms products with a structure or composition different from that of the host mineral, including the term in petrology “epitaxial overgrowth”, or forms small multinuclear inorganic complexes such as dimers or trimers; (iv) coprecipitation or substitution, which is to integrate solute species into the mineral structure through the dissolution and re-precipitation of the mineral, or through lattice diffusion and isomorphic substitution within the mineral lattice (Krauskopf and Bird, 1995). The general concepts of sorption, adsorption, and absorption are easily confused and need to be distinguished in order to identify potential risk of Cd release back into the soil pore water.

Adsorption is a two-dimensional process where the solute molecules or atoms (i.e., adsorptives) leave the solution and attach to the mineral surface (i.e., adsorbent). The molecules and atoms on the mineral surface (adsorbates) are bound via surface complexes, which can be divided into two types on the basis of the atomic arrangements and bonding properties between adsorbate and adsorbent. One of these arrangements is an outer sphere complex, which contains one or several water molecules between the mineral surface and the adsorbed species; outer sphere complexes are affected by weak electrostatic attractions. Another sorption mechanism is an inner sphere complex, which mainly forms a strong, short-range ionic bond or covalent bond at a characteristic crystal site without any water molecules between the adsorbed species and the mineral surface (Stumm and Morgan 1981; Sparks 1995). Inner-sphere complexes can be monodentate, bidentate, or tridentate depending on the surface site on the adsorbent (Fig. 1). This method of classification of bonding is based on a polyhedral approach to surface complexes.

Recent evidence for a continuous transition between surface complexation (adsorption) and surface precipitation indicates that as the amount of metal cations or anions adsorbed on the surface (surface coverage or surface loading) increases to a higher surface coverage, surface precipitates may form (Siebecker *et al.*, 2014) (Fig. 1). The traditional way to view surface precipitation is that at low surface loading, surface complexation tends to dominate. As surface loading increases, surface polymers or multinuclear surface complexes may form with further nucleation occurring on the surface. As surface coverage increases further, surface precipitation becomes the predominant mechanism. In addition to this view, it has also been shown that surface precipitation can occur at surface coverage of below 5% (Scheidegger *et al.*, 1996).

Sorption is one of the most significant chemical processes in soil systems. It determines the quantity of plant nutrients, metals, radionuclides, pesticides, and other organic chemicals that are retained on soil surfaces. Hence, it is one of the key processes that affects migration of nutrients and contaminants in soils. Sorption also affects the electrostatic properties of suspended particles and colloids, which have an influence on coagulation and settlement (Stumm 1992; Sparks 1995).

In certain cases, surface incorporation (substitution of atoms into a mineral surface) would occur at a dynamic surface. For example, when Cd^{2+} was sorbed on birnessite in the presence of dissolved Mn^{2+} , an interface coupled dissolution-precipitation (ICDP) process took place, causing a rapid atomic exchange of the aqueous Mn^{2+} and the surface Mn atom of birnessite. This exchange induced the incorporation of Cd^{2+} into the mineral during its sorption at birnessite-solution interface (Sun *et al.*, 2019). Because these mechanisms only exhibited structural differences at the molecular scale, a spectroscopic technique was needed to distinguish them. One of the most widely applied spectroscopic technique is X-ray absorption spectroscopy (XAS).

3. BRIEF INTRODUCTION OF X-RAY ABSORPTION SPECTROSCOPY

X-ray absorption fine structure spectroscopy (XAFS) is an advanced structural analysis technique based on a synchrotron radiation X-ray source. This section gives a brief introduction to the general theoretical concepts, facilities, experimental method, and data analysis. Other resources for the use of synchrotron X-rays for soils and geosciences are available (Kelly *et al.*, 2008; Calvin, 2013).

3.1 EXAFS and XANES

X-ray excited photoelectrons are scattered by the surrounding coordinating atoms, causing the X-ray absorption intensity to oscillate with energy. By studying these oscillating signals, one can obtain the electronic and geometric local structures of the studied system. One important distinction of XAS-based methods is that they are element-specific, meaning that a study can focus on a single element (e.g., Cd) in a heterogeneous media such as soils. XAS-spectra are usually divided into two regions: the extended X-ray absorption fine structure (XAFS or EXAFS) and the near edge fine structure (NEXAFS or XANES).

The XANES portion of the XAS spectrum, which is characterized by a continuous, sharp, strong rise, includes three detailed parts: (i) the pre-edge region arising from the transition of the “inner-core” electrons to the unoccupied bound states, (ii) the elemental absorption edge at the ionization energy, E_0 , which is in general the largest visible feature in the spectrum and whose position in energy increases with atomic number, and (iii) the region that is 50-100 eV above the elemental absorption edge, arising from the multiple scattering (MS) of the excited photoelectrons on the outlying neighboring atoms (Frank C., 1988). The XANES features mainly give the electronic structural information of the absorbing atom due to its sensitivity to the valence and neighbor coordination in a structure (Schulze and Bertsch, 1995). The acquisition of XANES spectrum is typically quick (from seconds to tens of minutes, depending on the experimental setup and sample), so the XANES analysis is suitable for time-resolved study. The spectral features seen in the XANES region are often given the term “fingerprint”. The simple "fingerprint" characteristics of XANES spectrum can be applied to identify the chemical species (e.g., valence states) quickly.

Unlike XANES, the EXAFS region is characterized by a continuous, gentle, weak oscillation. The energy range of the EXAFS region is up to about 800 eV above the absorption edge. The underlying principle of the EXAFS spectrum is that the incident X-ray photons are energetic enough to eject electrons completely from the absorber atom, and the excited photoelectrons are then coherently scattered by neighboring atoms. Over this energy region (i.e., 800 eV), the vibrational frequency is negatively correlated with the distance between the absorber atom and the neighboring atoms, as well as the amplitude is highly related to the ligand type and the coordination number (Schulze and Bertsch, 1995). Therefore, EXAFS analysis can provide molecular information about the coordination number and interatomic distances in the geometric local environment of an absorber atom. The shape of the EXAFS spectrum is related to the short-range-ordering (SRO) of several coordination shell atoms, which represent the nearest neighboring atoms around the element of interest (within 6 Å) (Brown and Parks, 1989), thus the spectra will change if a crystal structure changes. These scattering processes make EXAFS a complementary technique to X-ray diffraction, and it is suitable for probing local structure of poorly-crystalline material and sorbed species at solid-water interfaces. The critical aspects of these two environments are that they dictate elemental reactivity (i.e., adsorption/desorption reactions) and impact environmental fate of contaminants. Additionally, both of these environments lack long-range-ordering (LRO) structure, which is

typically probed using X-ray diffraction (XRD).

3.2 Synchrotron facilities and beamline setup

Synchrotron radiation facilities generally produce high energy and large fluxes of electromagnetic radiation (light). The combination of high energy and large flux means they are very “bright” sources of light. This light is produced when charged particles (i.e. electrons) move at velocities close to the speed of light in an ultra-high vacuum environment (e.g., a storage ring). Using a series of magnets, the electrons are forced to change direction around the ring, and when their direction of motion is forced to change, they emit radiation in the form light. For the purpose of a user to understand how a synchrotron facility is designed, there are three main components: booster ring, storage ring, and beamline (Fig. 2). Synchrotron radiation-based X-rays produced from an electronic storage ring are used during experimental operations. These X-rays possess a number of unique and excellent properties, such as a wide energy spectrum (e.g., several hundred eV up to >100 keV), high brightness (e.g., 1×10^{13} or higher photons per second), high stability, high polarized and time-structured emission. There are more than 70 synchrotron light sources around the world (operational, or under construction) (<https://lightsources.org/>), among which there are currently three synchrotron radiation sources in operation in mainland China, including Beijing Synchrotron Radiation Facility (BSRF), Hefei Light Source (HLS), and Shanghai Synchrotron Radiation Facility (SSRF). There are more than 10 light sources (under construction and/or operation) in the Americas.

Fig. 2 (A) Photograph and (B, C) Schematic of the Shanghai Synchrotron Radiation Facility (<http://ssrf.sinap.cas.cn/>).

The general experimental set-up of the detectors, optics and sample positioners used in the XAFS experiment at the beamline are shown in Fig. 3. There are five major parts to the set-up: (i) the X-ray source including the bending magnet or insertion device, which are both located in the electron storage ring, (ii) the optics including slits, mirrors and the monochromator, (iii) the sample and sample holder, (iv) the detectors, and (v) the amplifiers and computers. Several sets of mirrors can be used for various purposes. For example, focusing mirrors and slits can ensure the beam is approximately 1x5 mm in size for experiments where a “bulk” representation of the sample is

desired. However, in soils and environmental geochemical systems, mirrors can also be used to focus the X-ray beam to the micrometer scale. The purpose of analysis at the micrometer scale is to probe the chemical heterogeneity that one commonly finds in soils. Using a microfocused beamline, the scientist can identify less common but more reactive species in the sample that may not be observed from a bulk analysis. Regarding the sample setup, there are mainly two kinds of measurement geometries for bulk measurements. In the transmission mode, the transmission of X-rays is registered via the I_0 and I flux monitors (also termed “ionization chambers”). The quantity of X-rays absorbed by the sample can be measured and plotted as ratio of the natural logarithm I_0/I . In the fluorescence mode, the intensities of the fluorescence photons or secondary electrons emissions are detected while the sample is placed at a 45° to the incident X-ray beam.

Fig. 3 (A) Schematic diagram of a generic XAFS experimental beamline setup; The ring on the left represents the electron storage ring (booster ring not indicated). X-rays are produced tangential to the ring as electrons move around it. They are then focused and filtered via slits and monochromator. I_0 through I are located in the sealed (but accessible) experimental room called the “hutch”. The sample holder is often motorized and can be controlled from the computer outside the hutch. (B) Beamlines and Experimental stations in SSRF; (C) The “hutch” inside the sampling chamber of an XAFS beamline, BL14W1, in SSRF.

3.3 Sample preparation

XAFS measurements can be performed on solids, liquids, gasses, wet pastes, suspensions and even biological samples. XAFS can also be carried out for *in-situ* measurements of these samples at room temperature and atmospheric pressure, with the measurable concentration close to the environmental level (0.1wt%) (Brown *et al.*, 2005). This is particularly important for soils and environmental samples because trace metals, which are often environmentally hazardous, are often found at low concentration.

The quality of an XAFS spectrum often depends on the quality of sample preparation. Therefore, sample preparation and preservation are of utmost importance. For bulk XAFS measurements, a well-prepared sample should ensure that the speciation of the absorber atoms is well-preserved and uniformly distributed within the sample. Particle size of the sample should ensure that the element of

interest in bound to particles of less than one absorption length at the energy of interest. Additionally, the concentration of absorber element should be above the detection limit for the particular beamline. Different data collection modes may be required for different samples. Transmission mode is valid for samples containing the element of interest at concentrations greater than 5% weight, while fluorescence mode is advantageous for thin concentrated or thick dilute samples containing the element of tens to hundreds of ppm. The methods of sample preparation and containment depend on the sample properties. It is critical to understand the sample concentration and thickness so as to avoid production of artifacts in the raw data. Samples prepared improperly will result in unusable data.

Solid samples can be finely ground and uniformly smeared over the sticky side of a high-purity, heat resistant Kapton tape, while the sample thickness can be adjusted by folding the tape by several layers (Fig. 4C) (Melissa, 2006; Kelly *et al.*, 2008). Another practical way to prepare a powder sample is to disperse the sample (if necessary to reduce the concentration) in a diluting agent (e.g. boron nitride powder or poly ethylene glycol (PEG)) and press it into a pellet. PEG is often convenient because it helps the pellet stick together. Additionally, with the pellet press method, there is a known mass and diameter of the pellet, which can be useful for calculating the X-ray absorption coefficient. Pellets can be used for either transmission or fluorescent mode data acquisition, depending on sample composition. Liquid samples can be put into specialized sealed containers, with windows openings for incident and transmitted X-rays, while the sample path length can be adjusted with the variable volume. Additionally, liquid samples, depending on their composition, can be sealed in a vessel such as in Fig 4A. For moist paste samples, they are usually uniformly spread into the windows of the specialized sample holders (Fig. 4A, B), which is made of polymethyl methacrylate (PMMA) or Teflon of various thickness. Additionally, samples obtained from mineral slurries can be filtered and mounted on sample filters for analysis (Lafferty *et al.*, 2010).

Fig. 4 Common sample preparation methods used for collecting XAFS data. (A) and (B) represent plastic sample holders of various thickness where wet or dry samples can be mounted. (C) is folded Kapton tape with dry powder sample spreading evenly across the sticky surface of the tape and folded several times to avoid any pin-holes in the sample. (D) shows three metal pieces called a die that fit together and are used to form a pellet from a dry sample. The particular metal die has a diameter of 7 mm, thus allowing the user to create a

sample with a precisely weighted sample of known diameter for analysis at the beamline.

3.4 Data acquisition and processing

The energy dependence of the X-ray absorption coefficient $\mu(E)$ can be measured either in transmission mode as $\mu(E) = \ln(I_0/I)$, or in fluorescence mode as $\mu(E) \propto I_f/I_0$, where I_0 is the detected intensity of the incident X-rays, I is the intensity of the monitored transmitted X-rays, and I_f is the detected intensity of the fluorescence X-rays emitted from the sample, which are proportional to the absorption process. Data are generally calibrated using a known reference material, for example, a metal foil.

For both XANES and EXAFS data analysis, the initial step in the data reduction process is pre-edge background subtraction and normalization of the edge step value from the raw. The data are normalized to a 0 to 1 scale, which permits comparison of spectra from samples of different concentrations. Then either XANES or EXAFS spectra can be obtained from the raw XAFS data (Fig. 5). The XANES portion is simply to be obtained by adjusting the energy range to the appropriate range (Fig. 5B). Generally the XANES region is from -20 to +50 eV from the absorption edge, but can vary slightly depending on the specific needs of the user. Data processing of EXAFS portion is more complicated than for XANES. The EXAFS data processing steps can be divided into several steps. (i) The post-edge data should be background subtracted to remove $\mu_0(E)$, which represents the absorption coefficient in the absence of neighboring atoms (Fig. 5C). (ii) Convert the energy axis to photoelectron wave vector, i.e., k , through the following equation:

$$k = \sqrt{\frac{2m_e}{\hbar^2} (E - E_0)},$$
 where m_e is the mass of an electron, \hbar is the Planck's constant divided by 2π , and E is the incident X-ray energy.

(iii) Weight the higher- k portion of the spectra, where the amplitude of the EXAFS oscillations decays rapidly with increasing k . The purpose of weighting the spectra is to amplify the oscillations, which contain structural information. Normally the data are multiplied by a factor of k^2 or k^3 (Fig. 5D). (iv) A Fourier transform (FT) is performed in order to filter out the frequency and amplitude of different oscillations which compose the EXAFS data. The

FT changes the data from wave vector (k) space into the radial structure function (R) space, which is a way of directly viewing interatomic scattering distances in term of Angstroms. The scattering contribution from each shell to the EXAFS oscillations is decomposed and can be viewed as independent peaks (Fig. 5E). In the R-space (Fig. 5E), the positions of the peaks are correlated with the atomic distances (but do not account for phase shifts), while the intensities of the peaks are correlated with the coordination numbers. The intensity of the peak is also affected by constructive and destructive interference of scattering photoelectric waves. Thus, constructive interference will increase the amplitude of the peak in the FT while destructive interference the opposite.

Fig. 5 The basic steps of XAFS data reduction. (A) Measured experimental raw spectra of an aqueous Cd solution and solid Cd(OH)₂ reference compounds, collected in transmission modes; (B) normalized, background subtracted absorption spectra on a 0 to 1 scale; (C) k^3 -weighted EXAFS spectra extracted from the raw data; (D) magnitude of Fourier transform of EXAFS data; (E) normalized, background subtracted XANES spectra, ranging from -50eV to +100eV from the edge.

After these data reduction steps, there are mainly two types of data analysis methods for EXAFS data, the choice of which will depend on the specific experimental objectives and set up. One of the methods is a statistical quantitative analysis called linear combination fitting (LCF), and the other is a structural refinement method generally called “shell-by-shell fitting”. In LCF, the spectra for an unknown sample is compared to multiple spectra for well characterized samples. This method can be used for both XANES and EXAFS analysis. For shell-by-shell fitting, the peaks seen in the FT (Fig. 5D) are calculated using theoretical scattering paths based on a structural model. If the structural model used to fit the data is accurate, then the statistical results for each of the fitted EXAFS variable will be physically reasonable, thus indicating a good fit. The shell-by-shell method can be used to obtain the information of interatomic distances and coordination numbers.

4. XAFS STUDIES ON THE SORPTION MECHANISM OF CD(II) AT SOIL MINERAL SURFACES

The speciation of divalent Cd in aqueous solutions is dominantly as a hexahydrate cation ($\text{Cd}(\text{H}_2\text{O})_6^{2+}$); this is true for Cd at low concentration (e.g., $<0.1\text{M}$) and at acidic and weakly alkaline pH ranges (e.g. pH 2~8). At higher pH, Cd is present as mononuclear ($\text{Cd}(\text{OH})_n^{(2-n)+}$ ($n=1-4$)) as hydrolysis products are formed at higher pH (e.g. pH ≥ 8). In concentrated Cd(II) solutions, multinuclear hydrolysis products ($\text{Cd}_2\text{OH}^{3+}$, $\text{Cd}_4(\text{OH})_4^{4+}$) start to form in small amounts during hydroxide precipitation (Baes and Mesmer, 1986; Bochatay and Persson, 2000). In solution, Cd(II) is generally six-coordinated by oxygen, i.e. octahedral coordination (Greenwood and Earnshaw, 1984). Occasionally, Cd(II) can also exhibit higher coordination numbers ranging from 8 to 12 owing to its longer average ionic radius (i.e., 0.95\AA) when coordinated by six oxygens in solids as compared with 0.70\AA for $^{\text{VI}}\text{Ni}(\text{II})$, 0.73\AA for $^{\text{VI}}\text{Cu}(\text{II})$, 0.735\AA for $^{\text{VI}}\text{Co}(\text{II})$, and 0.745\AA for $^{\text{VI}}\text{Zn}(\text{II})$ (Shannon, 1976).

There have been a number of macroscopic batch and spectroscopic studies of Cd(II) sorption on several sorbents, including iron hydroxides (Spadini *et al.*, 1994; Randall *et al.*, 1999; Manceau *et al.*, 2000), aluminum oxides (Papelis, 1995; Papelis *et al.*, 1995; Sun *et al.*, 2019), manganese (hydr)oxides (Randall *et al.*, 1998; Bochatay and Persson, 2000; Sun *et al.*, 2018), and (alumino)silicates (Farquhar *et al.*, 1997; Gräfe *et al.*, 2007; Vasconcelos *et al.*, 2008). In all cases, Cd(II) was found to be six-coordinated by oxygen. As discussed below, there are four possible mechanisms for Cd(II) removal from the solution phase via interaction with these mineral surfaces, namely: (i) outer-sphere surface complexation, (ii) inner-sphere surface complexation, and (iii) precipitation, and (iv) ion exchange. Of these four mechanisms, inner-sphere complexation has been observed in all of these systems, particularly in the systems of Fe/Mn (hydr)oxides. Precipitation of Cd-rich solids has mainly been observed in the systems of aluminum oxides, whereas outer-sphere complexation has mainly been observed in the systems of (alumino)silicates. The ion exchange mechanism has occasionally been observed in the systems of some minerals with interlayer or tunnel structure, such as biotite and cryptomelane.

4.1 Iron oxides

The sorption of Cd^{2+} on ferric hydroxides, including hydrous ferric oxide (HFO), goethite ($\alpha\text{-FeOOH}$), and lepidocrocite ($\gamma\text{-FeOOH}$), has been studied by XAFS spectroscopy (Spadini *et al.*, 1994; Randall *et al.*, 1999; Manceau *et al.*, 2000). The EXAFS study by Spadini *et al.* (1994) showed

that Cd atoms sorb on goethite by both sharing edges and corners with surface Fe octahedra at surface coverage from 11% to 100% and form mainly double-corner-sharing complexes (or referred as bidentate binuclear surface complex) as surface coverage increases, i.e. under conditions of moderate to high Cd surface loading. The investigation by [Randall *et al.* \(1999\)](#) also provided evidence for expected corner-sharing surface complexes on goethite over a wide range of pH and at higher surface loadings, consistent to the results of [Spadini *et al.* \(1994\)](#). The EXAFS data from [Randall *et al.* \(1999\)](#) suggested that the goethite morphology inhibited Cd sorption at edge-sharing sites owing to the fairly low proportion of edge-sharing sites (~2%) than corner-sharing sites on goethite surfaces; although their quantum mechanical modeling indicates that the edge sharing adsorption is more energetically favorable than corner sharing adsorption. [Randall *et al.* \(1999\)](#) also indicated the sorption mechanism of Cd on lepidocrocite by mainly via sharing edges with surface Fe octahedra, distinctly different to goethite, and was interpreted as being due to the far greater proportion of edge-sharing site than goethite. However, this explanation is refuted by [Manceau *et al.* \(2000\)](#) based on the calculation of surface site densities performed, which showed that there are not enough edge-sharing surface sites available for the sorbed Cd on lepidocrocite crystallites. This difference found by [Manceau *et al.* \(2000\)](#) was further interpreted by the different bulk structures and the stacking mode of anion layers (O^{2-} , OH^-) which is hexagonal in goethite and cubic in lepidocrocite.

In addition, Cd(II) was found to prefer higher affinity sites (i.e., edge-sharing sites) on HFO than on α -FeOOH by [Spadini *et al.* \(1994\)](#). Considering all these bonding environments, the dominant mechanism of Cd(II) adsorption on iron oxides is inner-sphere surface complexation, irrespective of edge-sharing or corner-sharing. According to the ab initio calculation results and the predicted geometries of molecular clusters ([Fig. 6](#)) for Cd on goethite by [Randall *et al.* \(1999\)](#), edge-sharing bindings were characterized by significantly shorter Cd-Fe distances (2.87-3.34 Å) than corner-sharing bindings (3.52-3.76 Å). The Cd-Fe distance in single corner-sharing structure (3.52 Å) also is relatively shorter than that in double corner-sharing structure (3.76 Å). The geometries of Cd sorption on iron oxides derived from EXAFS data in the previous studies ([Table 1](#)) were essentially consistent with this prediction model: the first shell Cd-O distances of inner-sphere complexes are similar and range from 2.24-2.30 Å, whereas the second shell Cd-Fe distances of edge-sharing complexes (3.26-3.32 Å) are considerably shorter than corner-sharing complexes (3.48-3.80 Å).

Fig. 6 Crystal structure of goethite (A, B); Optimized geometries for DFT-optimized clusters representing Cd(II) adsorption complexes on goethite, reproduced from Randall *et al.* (1999) with copyright permission from Elsevier (C~F).

4.2 Manganese oxides

The sorption of Cd^{2+} on manganese (hydr)oxides, including cryptomelane (KMn_4O_8), manganite ($\gamma\text{-MnOOH}$), $\delta\text{-MnO}_2$, has also been studied (Randall *et al.*, 1998; Bochatay and Persson, 2000; Sun *et al.*, 2018). The study of Cd^{2+} sorption on cryptomelane by Randall *et al.* (1998) suggested that Cd^{2+} is preferentially sorbed within the tunnel sites through charge-balancing exchange with H^+ . Bochatay *et al.* (2000) suggested the formation of six-coordinated Cd(II) edge-sharing inner-sphere complexes at the water-manganite interface. With respect to birnessite, the most common Mn oxide in the environment, most studies focused too much on the sorption behavior of Cd(II) on birnessite surfaces, while neglected the molecular binding mechanisms and the impact of coexisting reductive ions such as Fe(II) and Mn(II). A combined powder X-ray diffraction (XRD) and X-ray photoelectron spectroscopy (XPS) study revealed that Cd(II) was adsorbed mainly at the vacancy sites in the interlayer of hexagonal birnessite according to the relationship between Cd(II) sorption behavior and Mn average oxidation state (Wang *et al.*, 2012). A differential pair distribution function (d-PDF) analysis carried out by van Genuchten and Peña (2016) demonstrated that Cd(II) was adsorbed mainly on the cation vacancy (internal) sites, while a small portion of Cd(II) bound to birnessite particle edge (external) sites. A more recent combined XPS, XRD and EXAFS study by Sun *et al.* (2019a) investigated the effect of Mn(II) on Cd^{2+} sorption on $\delta\text{-MnO}_2$ and Mn(III)-rich $\delta\text{-MnO}_2$. This study revealed that in the absence of Mn(II), Cd forms mainly triple-corner sharing (TCS) inner-sphere complexes at Mn(IV) vacant sites with a minor amount of double-corner sharing (DCS) complexes at Mn(IV) edge sites on the $\delta\text{-MnO}_2$ surfaces; however it forms double-corner sharing (DCS) and double-edge sharing (DES) complexes with Mn(III) edge sites on Mn(III)-rich $\delta\text{-MnO}_2$. In the presence of Mn(II), Mn(II) competes for the sorption sites with Cd(II), inducing partial Cd(II) migration from vacant sites to less stable edge sites at low Mn(II) concentration under either acidic or alkaline conditions (Fig. 7). While at higher pH and Mn(II) concentration, Mn(II) would react with birnessite, leading to the formation of amorphous Cd(II)-Mn(III) coprecipitate. In

the manganese oxides systems, similar to iron oxide systems, the Cd-Mn distance of an edge-sharing complex derived from second-shell analysis varies from 3.20 Å to 3.37 Å, whereas the Cd-Mn distance indicating an corner-sharing complex varies from 3.66 Å to 3.76 Å (Table 1).

Fig. 7 Cd(II) immobilization mechanisms by birnessite inferred from EXAFS results. From Sun et al. (2019a), with copyright permission from Elsevier.

4.3 Aluminum-rich minerals

The sorption of Cd²⁺ on Al-bearing minerals, including Al (hydro)oxides (e.g., alumina, gibbsite), and aluminosilicates (e.g., kaolinite, feldspar, mica), has been studied by XAFS spectroscopy (Papelis, 1995; Papelis *et al.*, 1995; Farquhar *et al.*, 1997; Gräfe *et al.*, 2007; Vasconcelos *et al.*, 2008; Sun *et al.*, 2019b). In systems involving aluminosilicates, outer-sphere complexed Cd(II) species occurred. According to studies by Gräfe *et al.* (2007) and Vasconcelos *et al.* (2008) in the kaolinite system, outer-sphere surface complex formed at low pH (e.g. pH<7) and inner-sphere surface complexes at higher pH (e.g. pH 9) (Fig. 8). In the XAFS study of Cd²⁺ sorption on perthite, biotite, feldspar and muscovite (Farquhar *et al.*, 1997), it was suggested that Cd(II) forms only outer-sphere complexes on perthite, feldspar and muscovite, whereas Cd(II) was thought to form stronger surface complexes on biotite possibly as inner-sphere complexes coupled with some ion exchange.

Fig. 8 Simplified graphical presentations of outer sphere Cd complexes at the kaolinite–water interface, and inner sphere complexes on gibbsite. From Gräfe *et al.* (2007), with copyright permission from Elsevier.

In systems with Al (hydro)oxides, Cd(II)-containing precipitates were also reported in addition to surface complexes. According to Papelis *et al.* (1995), Cd(II) was sorbed on Al oxides mainly as mononuclear surface complexes and formed a disordered Cd hydroxide or Cd hydroxocarbonate precipitate at higher Cd(II) concentration (10⁻³ M). The first shell Cd-O distance was 2.35 Å and the second shell was Cd-Cd of 3.84 Å. Owing to the much larger radius of Cd²⁺ (0.97 Å) than that of Al³⁺ (0.54 Å), Cd had not been shown to form LDH via surface sorption on Al-bearing minerals (Papelis, 1995; Papelis *et al.*, 1995; Vasconcelos *et al.*, 2008; Gräfe *et al.*, 2007; Papelis, 1995),

differing from Ni^{2+} , Zn^{2+} , and Co^{2+} as discussed in previous studies (Delacaille *et al.*, 1995; Scheidegger *et al.*, 1996, 1998; Towle *et al.*, 1997; Scheinost *et al.*, 1999; Thompson *et al.*, 1999; Scheinost and Sparks, 2000; Ford and Sparks, 2000; Nachtegaal and Sparks, 2004; Li *et al.*, 2012; Gou *et al.*, 2018). However, a recent study by Sun *et al.* (2019b) confirmed the thermodynamic feasibility of Cd-Al LDH formation by laboratory synthesis of Cd-Al LDH and DFT calculations. They identified the formation of Cd-Al LDH on $\gamma\text{-Al}_2\text{O}_3$ by linear combination fitting (LCF) analysis of EXAFS data and XRD.

5. NEW METHODS FOR PROBING CD SORPTION MECHANISMS AT SOIL INTERFACES

5.1 Solid-state nuclear magnetic resonance spectroscopy

In addition to XAFS spectroscopy, solid-state nuclear magnetic resonance (NMR) is also an effective technique to obtain the information on the bonding and chemical environment of an adsorbed species at environmental mineral/water interfaces. The ^{113}Cd NMR method is indeed sensitive and effective because the ^{113}Cd isotope possesses (i) a filled d orbital, so that its coordination geometry is not impacted by the ligand field effect; (ii) a spin of $1/2$, which means no quadrupolar contribution to NMR relaxation and the NMR signal maintains a narrow width; (iii) a relatively high natural abundance of 12.26%; and (iv) an observed chemical dispersion of $>900\text{ppm}$ (Ellis, 1983).

Several studies utilizing solid-state NMR spectroscopy have investigated the interaction between Cd and layered silicates in detail, especially the Cd-smectite interaction. Bank *et al.* (1989) applied ^{113}Cd magic-angle spinning (MAS) NMR to study Cd-exchanged montmorillonite at pH 7 and observed one peak with chemical shift $\sim 15.6\text{ppm}$. The spectrum was simulated with two components with different peak widths, which were interpreted as due to the heterogeneity of the Cd adsorption sites. Edge sites which were more specific and likely to involve a permanent charge gave the narrower signal with a peak width of 1 kHz, and interlayer sites where nonspecific adsorption could occur and were closer to Fe in the octahedral sheets gave the broader signal with a peak width of 6-9 kHz. In contrast with the conclusions of Bank *et al.* (1989), Tinet *et al.* (1991) also studied ^{113}Cd NMR peaks with two components and interpreted them as the anisotropy of signal due to interaction between interlayer Cd and hydroxyl groups in the hexagonal cavities, instead of the effect

of multisite or different chemical environment.

Jun *et al.* (1996) investigated the interaction between montmorillonite and aqueous CdCl₂ solution ([CdCl₂] = 4.11 × 10⁻² M) and recorded a single peak at chemical shift of δ -8 ppm of the sedimented montmorillonite using ¹¹³Cd MAS NMR, indicating only free Cd²⁺ is selectively adsorbed on the negatively charged solid surface. Consistent with the results of Jun *et al.* (1996), Di Leo and O'Brien (1999) also observed one resonance peak at ~10ppm in the MAS NMR spectra, indicating there is only one site for Cd²⁺ sorption on montmorillonite at low Cd concentration ([CdCl₂] = 0.1 M). While at high Cd concentration ([CdCl₂] = 1 M), three components were detected and interpreted as a combination of Cd²⁺ in the interlayer (~10ppm), Cd²⁺ on the external surface sites (~ -40ppm), and CdCl⁺ in the interlayer (~116ppm) (Fig. 9). Though, it should be noted that such high concentrations of Cd would not be found in a soil solution. Furthermore, Sullivan *et al.* (1998, 2000) performed ²⁷Al-¹¹³Cd spin-echo double-resonance (SEDOR) and 2D-exchange NMR experiments to study the Cd-smectite binding and the mobility of the cations. They demonstrated that Cd was rigidly bound inside the pseudo-hexagonal cavities of the tetrahedral sheet in the dehydrated Cd-smectite. This was determined because otherwise ²⁷Al-¹¹³Cd coupling would not have been observed due to the rather long distance between the interlayer Cd and the Al atoms in the octahedral sheet (>5Å). More recently, Di Leo and Cuadros (2003) combined ¹¹³Cd and ¹H MAS NMR spectroscopy with Fourier transform infrared (FTIR) spectroscopy to investigate the chemical environment of Cd species on the surfaces of both dioctahedral and trioctahedral smectites, i.e., montmorillonite and hectorite respectively. This study confirmed that when the Cd concentration is sufficiently low and close to that of surface waters and groundwaters, Cd²⁺ is adsorbed on smectite mainly in the interlayer and surrounded by water molecules. This study also indicated that in smectites with no tetrahedral substitution, Cd occupies a single site in the center of the interlayer along the c axis due to symmetrical attraction from sheets on both sides, whereas in smectites with tetrahedral substitution, the Cd atoms interact more strongly with the basal oxygen atoms in the tetrahedral sheet. This is because the substitution in the sheet provide excess negative charge, causing a second site in addition to occupying the center of the interlayer.

Fig. 9 ¹¹³Cd MAS spectra of 1 M CdCl₂-treated montmorillonite ((a) Westone A; particle size mode 12.85 μm; (b) Westone B; particle size mode 8.45 μm). Peak A: average value 116 ppm; Peak B: average value -11 ppm;

Peak C: average value -41 ppm. Reproduced from Di Leo and O'Brien (1999) with copyright permission from Clays and Clay Minerals.

5.2 Molecular simulations

Molecular simulations (MD) involving first-principles (i.e. ab initio) methods that is based on density functional theory (DFT) is another practical alternative which provides critical insight into understanding the fundamental mechanisms controlling the thermodynamics and kinetic processes at the mineral-water interface. MD is usually used to assist and complement the interpretation of spectroscopies, such as EXAFS data.

Randall *et al.* (1999) used ab initio molecular dynamics (AIMD) to optimize the geometries and relative stabilities of four small molecular clusters, i.e., four types of cadmium surface complexes (double corner sharing; single corner sharing; double edge sharing; single edge sharing) on goethite. The results showed the predicted Cd-Fe distances: double edge (2.87-3.34 Å), single edge (3.17 Å), single corner (3.52Å) and double corner (3.76Å). This study also calculated the relative total free energies of formation: double corner (0 kJ/mol⁻¹), single edge (-115 kJ/mol⁻¹), double edge (-309 kJ/mol⁻¹), which suggests the order of increasing cluster stability and supports the widely held theory that edge sharing adsorption is more energetically favorable than corner sharing adsorption.

Zhang *et al.* (2016) conducted systemic first-principles molecular dynamics (FPMD) simulations to model the stable complexes of Cd(II) adsorbed on (010) and (110) interfaces of a neutral 2:1 phyllosilicate framework (i.e. pyrophyllite) and obtained the microscopic structures and complex free energies for the three possible binding sites ($\equiv\text{SiO}$, $\equiv\text{Al}(\text{OH})_2$, $\equiv\text{AlOH}\equiv\text{AlSiO}$, and vacant sites, corresponding to monodentate, bidentate and tetradentate complexes respectively). The results showed the Cd-O distances and the desorption free energies on (010) interface: $\equiv\text{SiO}$ (2.13 Å, 5.4 ± 0.7 kcal/mol), $\equiv\text{Al}(\text{OH})_2$ (2.21~2.22 Å, 8.7 ± 1.0 kcal/mol), and vacant sites ($2.91\sim 2.96$ Å_{apical} and $2.21\sim 2.22$ Å, 16.8 ± 2.0 kcal/mol) (Fig. 10). Similar results for the (110) terminations were also found, suggesting that the vacant sites are the most favorable and stable bonding sites. On the basis of the above study that was simulated at room temperature (300K), Zhang *et al.* (2018) further carried out FPMD simulations at elevated temperature (423K), under which conditions surface complexation of divalent and trivalent cations were promoted significantly. The results showed the average Cd-O distances and the desorption free energies on (010) interface: $\equiv\text{SiO}$ (2.17 Å, 6.3 ± 0.3 kcal/mol),

$\equiv\text{Al}(\text{OH})_2$ (2.25 Å, 9.6±0.5 kcal/mol), and vacant sites (2.91 Å_{apical} and 2.24 Å, 16.3±0.9 kcal/mol). The main conclusions deduced from this study with respect to the surface complex structures, free energies and pK_a values, were that they were all are similar to those of Zhang *et al.* (2016). Additional simulations indicated that multinuclear surface complexes of Cd(II) hold stably at 423 K, and those multinuclear phases may act as precursors for epitaxial growth of new mineral phases.

Fig. 10 The equilibrium structures of Cd(II) complexes adsorbed on three binding sites on the (010) type interface of neutral framework 2:1 phyllosilicates. (A) $\equiv\text{SiO}$ site, (B) $\equiv\text{Al}(\text{OH})_2$ site, and (C) vacant site. The vacant site here is on the edge of the phyllosilicate mineral; however, it represents a vacant site where Cd can bind to 2 Al atoms. For clarity, the other water molecules have been removed. Solid parts are shown as sticks; Cd(II) and the coordinated water molecules are shown as ball-and-stick models. O = red (black), H = white (white), Si =yellow (gray), Al = purple (dark gray), and Cd = gold (light gray) with grayscale in parentheses. Reproduced from Zhang *et al.* (2016) with copyright permission from Clays and Clay Minerals.

6. IMPLICATIONS FOR SOIL REMEDIATION

Over the past forty years, immobilization or stabilization with mineral-based materials to reduce the leachability and/or bioavailability of heavy metals in contaminated soils is gaining acceptance as a widely applied *in-situ* remediation technology. Naturally-occurring rock-forming minerals that possess high specific surface area and provide countless bounding sites that have a strong affinity for metal ions have been shown to play an important role in effectively stabilizing heavy metal contaminants in soils (Berti and Cunningham, 1997; Chen *et al.*, 2000; Garcia-Sanchez *et al.*, 1999; Lothenbach *et al.*, 1997). According to our literature review, Al-bearing minerals, especially aluminum oxides, are expected to act more effectively than iron oxides and manganese oxides for reducing Cd mobility. This is because surface precipitation, which occurs commonly in the systems of Al-bearing minerals but rarely appears in the systems of Fe- and Mn- oxides, is a relatively valid sequestration mechanism owing to the stable three-dimensional local structure of precipitates. It can thus be reasonably assumed that Al-bearing minerals may be more applicable to amending Cd-contaminated soils, in terms of both the types of sorption products and long-term stability. Furthermore, from the perspective of economic cost of soil remediation, Al-containing clay minerals

show great potential for practical contaminated land remediation in a cost-effective and environmentally friendly manner. However, there is still a lack of knowledge about Cd sorption mechanisms on clay minerals, so that more comprehensive and systematic in-depth studies are needed for better decisions on soil remediation.

Furthermore, because of the high degree of diversity and heterogeneity of contaminated soils, there is no “one-size-fits-all” methodology in remediation approach. Another long-standing challenge in soil remediation is the unknown or unexpected long-time risk after remediation. This requires more precise control to the long-term fate and transport of trace metal contaminants in the complicated subsurface environment. In this regard, fundamental research on the mechanisms of metal sorption reactions at the soil mineral-solution interface in soil, environmental, and geochemical sciences is not only important but also indispensable. Without such knowledge, on the one hand, it could be unable to understand the metal speciation in soils, to make feasible and cost-effective strategies that can be applied to the field scale remediation, and then to establish complete risk assessment models. On the other hand, the speciation of trace metals in natural soil systems is complex, especially for samples with inherently low background concentrations, to be limited for characterization. Since the complex soil system is a microcosm and can be considered as an aggregation of innumerable single minerals, systematic exploration of molecular scale sequestering of trace metals by soil minerals such as iron oxides, manganese oxides, and aluminum-containing minerals (i.e., aluminum oxides and phyllosilicates) may provide necessary references and basis for the further understanding of the complicated system. Therefore, this review takes Cd(II), one of the most typical heavy metal contaminants in soil, as an example to summarize the Cd sorption mechanisms at the mineral/water interfaces, aiming to provide molecular theoretical foundation for predicting the mobility of trace metals and then for soil remediation.

7. SUMMARY AND PERSPECTIVE

Sorption of Cd at soil mineral/water interfaces is a complex process, which depends on pH, concentration and especially mineral type. However, as an important toxic metal contaminant, the environmental soil chemistry of Cd is still not well understood, and this topic needs more research to better predict Cd mobility in the environment. Here, we underscore several areas that worth further exploration.

First and foremost, most of the reported molecular level studies were based on laboratory research (Watts *et al.*, 2019); thus, the results of these studies, while important to understand fundamental adsorption and surface precipitation mechanisms, may not be directly applicable to the fields where Cd concentrations are much lower (ppm level). Thus, future studies should focus more on natural samples with lower Cd concentrations. As discussed above, the current synchrotron light sources only allow a sample concentration down to a few hundred ppm to be adequately characterized, which is still higher than many soil environments. An update of the current beamline facilities, which can provide higher fluxes and better sensitivity, may be necessary.

Besides, as a heavy element, the chi space of Cd EXAFS spectrum (for any of the above discussed sample) is usually dominated by the oscillation of first Cd-O shell, which would significantly suppress the signals contributed from further shells. This intrinsic limitation may raise great challenge to characterize a sample with presence of a mixture phases. To solve this problem, it requires development of more complementary techniques such as a combination of DFT_MD simulation and FEFF calculation of Cd L-edge XANES (Watts *et al.*, 2019).

Over the past decade, applications of metal stable isotopes in environmental science became a promising research direction. The cadmium stable isotope is an excellent tool to track the source of Cd pollution and provide new insights into the fate of Cd in plant-soil systems (Wiggenhauser *et al.*, 2016). Currently, most reported $\delta^{110}\text{Cd}$ isotopic compositions has mainly focused on natural rock samples to decipher geological records while measurements of soil chemical process are sparse (Li *et al.*, 2019). This means that establishment of a stable isotope tracing protocol to investigating metal sorption process is feasible (Schauble, 2004; Gou *et al.*, 2018), which will offer new opportunities for environmental soil interface chemistry of Cd (Horner *et al.*, 2011; Wasylenki *et al.*, 2014).

ACKNOWLEDGEMENTS

This research was funded by the National Natural Science Foundation of China (Grant Nos. 41722303, 41977267, 41473084) and National Key R&D Program of China (2017YFD0800303). Special thanks for the financial support of the Opening Fund of State Key Laboratory of Environmental Geochemistry (SKLEG2019712) and the 1000 Youth Talent Program sponsored by the Chinese central government.

References

- Baes C F, and Mesmer R E. 1986. *The Hydrolysis of Cations*. John Wiley & Sons Inc., New York.
- Bank S, Bank J F, Ellis P D. 1989. Solid-state cadmium-113 nuclear magnetic resonance study of exchanged montmorillonites. *J. Phys. Chem.* **93**: 4847-4855.
- Berti W R, Cunningham S D. 1997. In-place inactivation of Pb in Pb-contaminated soils. *Environ. Sci. Technol.* **31**: 1359–1364.
- Bochatay L, Persson P. 2000. Metal ion coordination at the water-manganite (γ -MnOOH) interface II. An EXAFS study of zinc(II). *J. Colloid Interface Sci.* **229**: 584-592.
- Bolan N, Mahimairaja S, Kunhikrishnan A, Naidu R. 2013. Sorption–bioavailability nexus of arsenic and cadmium in variable-charge soils. *J. Hazard. Mater.* **261**: 725–732.
- Brown G E, Parks G A. 1989. Synchrotron-based X ray absorption studies of cation environments in earth materials. *Rev. Geophys.* **27**: 519-533.
- Brown G E, Catalano J G, Templeton A S, Trainor T P, Farges F, Bostick B C, Kendelewicz T, Doyle C S, Spormann A M, Revill K. 2005. Environmental interfaces, heavy metals, microbes, and plants applications of XAFS spectroscopy and related synchrotron radiation methods to environmental science. *Phys. Scr.* **T115**: 80-87.
- Calvin S. 2013. *XAFS for Everyone*. CRC Press, Boca Raton.
- Chaney R L. 2012. Food safety issues for mineral and organic fertilizers. *Adv. Agron.* **117**: 51–116.
- Chen H M, Zheng C R, Tu C, Shen Z G. 2000. Chemical methods and phytoremediation of soil contaminated with heavy metals. *Chemosphere.* **41**: 229–234.
- Chisholm-Brause C J, O'Day P A, Brown G E, Parks G A. 1990. Evidence for multinuclear metal-ion complexes at solid/water interfaces from X-ray absorption spectroscopy. *Nature.* **348**: 528-531.
- Delacailierie J B D, Kermarec M, Clause O. 1995. Impregnation of gamma-alumina with Ni(II) or Co(II) ions at neutral pH: hydrotalcite-type coprecipitate formation and characterization. *J. Am. Chem. Soc.* **117**: 11471–11481.
- Denecke M A. Actinide speciation using X-ray absorption fine structure spectroscopy. *Coord. Chem. Rev.* **250**: 730-754.
- Di Leo P, O'Brien P. 1999. Nuclear magnetic resonance (NMR) study of Cd²⁺ sorption on

- montmorillonite. *Clays Clay Miner.* **47**: 6164-6171.
- Di Leo P, Cuadros J. 2003. ^{113}Cd , ^1H MAS NMR and FTIR analysis of Cd^{2+} adsorption on dioctahedral and trioctahedral smectite. *Clays Clay Miner.* **51**: 403-414.
- Du H, Chen W, Cai P, Rong X, Dai K, Peacock C L, Huang Q. 2016. $\text{Cd}(\text{II})$ sorption on montmorillonite-humic acid-bacteria composites. *Sci. Rep.* **6**: 19499.
- Ellis P D. 1983. Cadmium-113 magnetic resonance spectroscopy. *Science.* **221**: 1141-1146.
- Farquhar M L, Vaughan D J, Hughes C R, Charnock J M, England K E R. 1997. Experimental studies of the interaction of aqueous metal cations with mineral substrates: lead, cadmium, and copper with perthitic feldspar, muscovite, and biotite. *Geochim. Cosmochim. Acta.* **61**: 3051-3064.
- Frank C. 1988. Spectroscopic Methods in Mineralogy and Geology, Reviews in Mineralogy. Mineralogical Society of America, Washington DC.
- Ford R G, Sparks D L. 2000. The nature of Zn precipitates formed in the presence of pyrophyllite. *Environ. Sci. Technol.* **34**: 2479-2483.
- Garcia-Sanchez A, Alastuey A, Querol X. 1999. Heavy metal adsorption by different minerals: Application to the remediation of polluted soils. *Sci. Total Environ.* **242**: 179-188.
- Gou W, Li W, Ji J F, Li W. 2018. Zinc isotope fractionation during sorption onto Al oxide: atomic level understanding from EXAFS. *Environ. Sci. Technol.* **52**: 9087-9096.
- Gräfe M, Singh B, Balasubramanian M. 2007. Surface speciation of $\text{Cd}(\text{II})$ and $\text{Pb}(\text{II})$ on kaolinite by XAFS spectroscopy. *J. Colloid Interface Sci.* **315**: 21-32.
- Greenwood N N, and Earnshaw A. 1984. Chemistry of the Elements. Pergamon Press, Oxford.
- Hayes K F, Roe A L, Brown G E, Hodgson K O, Leckie J O, Parks G A. 1987. In situ X-ray absorption study of surface complexes: selenium oxyanions on $\alpha\text{-FeOOH}$. *Science.* **238**: 783-786.
- Herzberg G. 1937. Atomic Spectra and Atomic Structure. Prentice-Hall, New York.
- Horner T J, Rickaby R E M, Henderson G M. 2011. Isotopic fractionation of cadmium into calcite. *Earth Planet. Sci. Lett.* **312**: 243-253.
- Hu Y, Cheng H. 2013. Application of stochastic models in identification and apportionment of heavy metal pollution sources in the surface soils of a large-scale region. *Environ. Sci. Technol.* **47**: 3752-3760.

- Järup L, Åkesson A. 2009. Current status of cadmium as an environmental health problem. *Toxicol. Appl. Pharm.* **238**: 201–208.
- Jun S, Chung K H, Moon C H. 1996. Adsorption of cadmium species on montmorillonite investigated by ^{113}Cd NMR spectroscopy. *Environ. Technol.* **17**: 655-660.
- Kabata-Pendias A, Pendias H. 2001. Trace Elements in Soil and Plants, 3rd edition. CRC Press, Boca Raton.
- Kelly S, Hesterberg D, Ravel B. 2008. Analysis of soils and minerals using X-ray absorption spectroscopy. In Ulery A, Drees L (ed.) Methods of soil analysis. Soil Science Society of America, Madison. pp. 387-463.
- Kossel W. 1920. Zum bau der röntgenspektren. *Zeitschrift für Physik.* **1**: 119-134.
- Krauskopf K B, Bird D K. 1995. Introduction to Geochemistry, 3rd edition. McGraw-Hill Inc, New York.
- Krishnamurti G S R, Huang P M, Van Rees K C J, Kozak L M, Rostad H P W. 1995. Speciation of particulate-bound cadmium of soils and its bioavailability. *Analyst* **120**: 659-665.
- Lafferty B J, Ginder-Vogel M, Zhu M, Livi K J T, Sparks D L. 2010. Arsenite oxidation by a poorly crystalline manganese-oxide. 2. Results from X-ray absorption spectroscopy and X-ray diffraction. *Environ. Sci. Technol.* **44**: 8467-8472.
- Li W, Luo L, and Zhang S. 2011. Towards a molecular scale understanding of the chemistry of inorganic ions at environmental interfaces: Application of spectroscopic techniques. *Progress in Chemistry.* **23**: 2576-2587.
- Li W, Livi K J T, Xu W, Siebecker M G, Wang Y, Phillips B L, Sparks D L. 2012. Formation of crystalline Zn–Al layered double hydroxide precipitates on γ -alumina: the role of mineral dissolution. *Environ. Sci. Technol.* **46**: 11670-11677.
- Li W, Gou W, Li W, Zhang T, Yu B, Liu Q, Shi J. 2019. Environmental applications of metal stable isotopes: Silver, mercury and zinc. *Environmental Pollution.* **252**: 1344-1356.
- Liu Y, Xiao T, Baveye P C, Zhu J, Ning Z, Li H. 2015. Potential health risk in areas with high naturally-occurring cadmium background in southwestern China. *Ecotoxi. Environ. Safe.* **112**: 122-131.
- Lothenbach B, Furrer G, Schulín R. 1997. Immobilization of heavy metals by polynuclear aluminum and montmorillonite compounds. *Environ. Sci. Technol.* **31**: 1452–1462.

- Luo L, Ma Y B, Zhang S Z, Wei D P, Zhu Y G. 2009. An inventory of trace element inputs to agricultural soils in China. *J. Environ. Manage.* **90**: 2524–2530.
- Manceau A, Nagy K L, Spadini L, Ragnarsdottir K V. 2000. Influence of anionic layer structure of Fe-oxyhydroxides on the structure of cd surface complexes. *J. Colloid Interface Sci.* **228**: 306-316.
- Nachtegaal M, Sparks D L. 2004. Effect of iron oxide coatings on zinc sorption mechanisms at the clay-mineral/water interface. *J. Colloid Interface Sci.* **276**: 13-23.
- National Research Council (NRC). 2003. Bioavailability of Contaminants in Soils and Sediments: Processes Tools, and Applications. National Academies Press, Washington DC.
- Nogawa K, Kido T. 1993. Biological monitoring of cadmium exposure in itai-itai disease epidemiology. *Int. Arch. Occup. Environ. Health.* **65**: S43–S46.
- Papelis C. 1995. X-ray photoelectron spectroscopic studies of cadmium and selenite adsorption on aluminum oxides. *Environ. Sci. Technol.* **29**: 1526-1533.
- Papelis C, Brown G E, Parks G A, Leckie J O. 1995. X-ray absorption spectroscopic studies of cadmium and selenite adsorption on aluminum oxides. *Langmuir.* **11**: 2041-2048.
- Randall S R, Sherman D M, Ragnarsdottir K V. 1998. An extended X-ray absorption fine structure spectroscopy investigation of cadmium sorption on cryptomelane (KMn₈O₁₆). *Chem. Geol.* **151**: 95-106.
- Randall S R, Sherman D M, Ragnarsdottir K V, Collins C R. 1999. The mechanism of cadmium surface complexation on iron oxyhydroxide minerals. *Geochim. Cosmochim. Acta.* **63**: 2971-2987.
- Satarug S, Garrett S H, Sens A, Sens D A. 2010. Cadmium, environmental exposure, and health outcomes. *Environ. Health Perspect.* **118**: 182–190.
- Schauble E A. 2004. Applying stable isotope fractionation theory to new systems. *Rev. Mineral. Geochem.* **55**: 65-111.
- Scheidegger A M, Lamble G M, Sparks D L. 1996. Investigation of Ni sorption on pyrophyllite: An XAFS study. *Environ. Sci. Technol.* **30**: 548-554.
- Scheidegger A M, Strawn D G, Lamble G M, Sparks D L. 1998. The kinetics of mixed Ni-Al hydroxide formation on clay and aluminum oxide minerals: a time-resolved XAFS study. *Geochim. Cosmochim. Acta.* **62**: 2233-2245.

- Scheinost A C, Ford R G, Sparks D L. 1999. The role of Al in the formation of secondary Ni precipitates on pyrophyllite, gibbsite, talc, and amorphous silica: a DRS study. *Geochim. Cosmochim. Acta.* **63**: 3193-3203.
- Scheinost A C, Sparks D L. 2000. Formation of layered single- and double-metal hydroxide precipitates at the mineral/water interface: a multiple-scattering XAFS analysis. *J. Colloid Interface Sci.* **223**: 167-178.
- Schulze D G, Bertsch P M. 1995. Synchrotron X-ray techniques in soil, plant, and environmental research. *Adv. Agron.* **55**: 1-66.
- Shannon R D. 1976. Revised effective ionic radii and systematic studies of interatomic distances in halides and chalcogenides. *Acta Crystallogr.* **32**: 751-767.
- Siebecker M, Li W, Khalid S, and Sparks D. 2014. Real-time QEXAFS spectroscopy measures rapid precipitate formation at the mineral–water interface. *Nat. Commun.* **5**: 5003.
- Smilde K W, Luit B, Driel W. 1992. The extraction by soil and absorption by plants of applied zinc and cadmium. *Plant Soil.* **143**: 233-238.
- Spadini L, Manceau A, Schindler P W, Charlet L. 1994. Structure and stability of Cd²⁺ surface complexes on ferric oxides: 1. Results from EXAFS spectroscopy. *J. Colloid Interface Sci.* **168**: 73-86.
- Sparks D L. 1995. Environmental Soil Chemistry. Academic Press, San Diego, CA.
- Stumm W. 1992. Chemistry of the Solid-Water Interface. John Wiley & Sons Inc., New York.
- Stumm W. and Morgan J J. 1981. Aquatic Chemistry. John Wiley & Sons Inc., New York.
- Sullivan D J, Shore J S, Rice J A. 1998. Assessment of cation binding to clay minerals using solid-state NMR. *Clays Clay Miner.* **46**: 349-354.
- Sullivan D J, Shore J S, Rice J A. 2000. ¹¹³Cd double-resonance NMR as a probe of clay mineral cation exchange sites. *Am. Mineral.* **85**: 1022-1029.
- Sun Q, Cu P, Fan T, Wu S, Zhu M, Alves M E, Zhou D, Wang Y. 2018. Effects of Fe (II) on Cd (II) immobilization by Mn (III)-rich δ-MnO₂. *Chem. Eng. J.* **353**: 167-175.
- Sun Q, Cui P, Zhu M, Fan T, Ata-Ul-Karim S T, Gu J, Wu S, Zhou D, Wang Y. 2019a. Cd(II) retention and remobilization on δ-MnO₂ and Mn(III)-rich δ-MnO₂ affected by Mn(II). *Environ. Int.* **130**: 104932.
- Sun Q, Liu C, Cui P, Fan T, Zhu M, Alves M E, Siebecker M G, Sparks D L, Wu T, Li W, Zhou D,

- Wang Y. 2019b. Formation of Cd precipitates on γ -Al₂O₃: Implications for Cd sequestration in the environment. *Environ. Int.* **126**: 234-241.
- The Ministry of Environmental Protection, The Ministry of Land and Resources. 2014. Report on the national soil contamination survey.
- Thompson H A, Parks G A, Brown G E. 1999. Dynamic interactions of dissolution, surface adsorption, and precipitation in an aging cobalt(II)-clay-water system. *Geochim. Cosmochim. Acta.* **63**: 1767–1779.
- Tinet D, Faugere A M, Prost R. 1991. ¹¹³Cd NMR chemical shift tensor analysis of cadmium-exchanged clays and clay gels. *J. Phys. Chem.* **95**: 8804-8807.
- Towle S N, Bargar J R, Brown G E, Parks G A. 1997. Surface precipitation of Co(II)_(aq) on Al₂O₃. *J. Colloid Interface Sci.* **187**: 62-82.
- van Genuchten C M, Peña J. 2016. Sorption selectivity of birnessite particle edges: a d-PDF analysis of Cd(II) and Pb(II) sorption by δ -MnO₂ and ferrihydrite. *Environ. Sci.: Processes Impacts.* **18**: 1030–1041.
- Vasconcelos I F, Haack E A, Maurice P A, Bunker B A. 2008. EXAFS analysis of cadmium(II) adsorption to kaolinite. *Chem. Geol.* **249**: 0-249.
- Wang P, Liu C, Yao Y, Wang C, Hou J. 2017. Comparison of *in situ* DGT measurement with *ex situ* methods for predicting cadmium bioavailability in soils with combined pollution to biotas. *Water Sci. Technol.* **75**: 2171-2178.
- Wang Y, Feng X, Villalobos M, Tan W, Liu F. 2012. Sorption behavior of heavy metals on birnessite: Relationship with its Mn average oxidation state and implications for types of sorption sites. *Chem. Geol.* **292**: 25–34.
- Wasylenki L E, Swihart J W, Romaniello S J. 2014. Cadmium isotope fractionation during adsorption to Mn oxyhydroxide at low and high ionic strength. *Geochim. Cosmochim. Acta.* **140**: 212-226.
- Watts H D, O'Day P A, Kubicki J D. 2019. Gibbsite (100) and kaolinite (100) sorption of cadmium(II): A density functional theory and XANES study of structures and energies. *J. Phys. Chem. A.* **123**: 6319-6333.
- Wen H, Zhang Y, Cloquet C, Zhu C, Fan H, Luo C. 2015. Tracing sources of pollution in soils from the Jinding Pb–Zn mining district in China using cadmium and lead isotopes. *Appl. Geochem.* **52**: 147-154.

- Wiggenhauser M, Bigalke M, Imseng M, Müller M, Armin Keller A, Katy Murphy K, Kreissig K, Rehkämper M, Wilcke W, Frossard E. 2016. Cadmium isotope fractionation in soil–wheat systems. *Environ. Sci. Technol.* **50**: 9223-9231.
- Zhang C, Liu X, Lu X, Meijer E J, Wang K, He M, Wang R. 2016. Cadmium (II) complexes adsorbed on clay edge surfaces: Insight from first principles molecular dynamics simulation. *Clays Clay Miner.* **64**: 337-347.
- Zhang C, Liu X, Lu X, He M. 2017. Complexation of heavy metal cations on clay edges at elevated temperatures. *Chem. Geol.* **479**: 36-46.
- Zhao X, Lu S, Xu R, Li B, Wu G, Wei F. 2014. Soil heavy metal cadmium standard limit and range of background value research. *Chin. J. Envir. Sci.* **35**: 1491-1497.

Table 1. Review of Cd sorption mechanisms on soil minerals

	Mineral	Approach	pH	Sorption mechanism	R _(Cd-O) (Å)	R _(Cd-Me) (Å)	Reference
Iron (hydr)oxides	Goethite (α -FeOOH)	EXAFS	7.5	Both edge- and corner-sharing inner-sphere complexes with surface Fe octahedra at the termination of goethite chains on (001) planes (at low coverage, i.e. Γ^a)=11 wt%); mainly corner-sharing complexes on (hk0) planes with Fe octahedral (at medium and high surface loading, i.e. Γ =65, 100 wt%)	2.30	R _{Fe1} = 3.26; R _{Fe2} = 3.48	Spadini <i>et al.</i> (1994)
	Hydrous ferric oxide (HFO)	EXAFS	6.7-9.5	Similar to goethite	2.27-2.30	R _{Fe1} = 3.32; R _{Fe2} = 3.50	Spadini <i>et al.</i> (1994)
	Goethite (α -FeOOH)	EXAFS	5.4-9.3	Bidentate inner-sphere surface complexes at corner sharing sites on the predominant (110) crystallographic surface	2.25-2.26	R _{Fe} = 3.75-3.80	Randall <i>et al.</i> (1999)
	Lepidocrocite (γ -FeOOH)	EXAFS	6.0-7.0 ^e)	Inner-sphere surface complexes at bi- and/or tridentate edge sharing sites	2.25-2.26	R _{Fe} = 3.26-3.30	Randall <i>et al.</i> (1999)
	Akaganeite (β -FeOOH),	EXAFS	8.0	Inner-sphere surface complexes	2.28	R _{Fe} = 3.29	Randall <i>et al.</i> (1999)

	Schwertmannite	EXAFS	6.5	Inner-sphere surface complexes	2.28	$R_{Fe} = 3.33$	Randall <i>et al.</i> (1999)
	Lepidocrocite (γ -FeOOH)	AFM, EXAFS	7.5	Mononuclear surface complexes on basal {010} and lateral {hk0}, {h0l} faces of lepidocrocite platelets by sharing edges with surface Fe octahedra	2.24-2.25	$R_{Fe} = 3.28-3.29$	Manceau <i>et al.</i> (2000)
Manganese (hydr)oxides	Cryptomelane (KMn_8O_{16})	EXAFS	2.0	Exchanged with H^+ in the tunnels rather than K^+ , partially hydrated.	2.24	$R_{Cd} = 3.65$	Randall <i>et al.</i> (1998)
	Manganite (γ -MnOOH)	EXAFS	7.4-9.8	Inner-sphere complexes, edge sharing between CdO_6 and MnO_6 octahedra ($\Gamma=2.2\sim 8.9\mu mol\ m^{-2}$)	2.30-2.33	$R_{Mn} = 3.32-3.37$	Bochatay and Persson (2000)
	δ -MnO ₂	XPS, XRD, EXAFS	5.5, 7.5	Both triple corner-sharing (TCS) complexes at vacant sites and double-corner sharing (DCS) complexes at edge sites	2.26	$R_{Mn} = 3.66$	Sun <i>et al.</i> (2019a)
	Mn(III)-rich δ -MnO ₂	XPS, TEM, EXAFS	5.5, 7.5	Double-corner sharing (DCS) and double-edge sharing (DES) complexes with Mn(III) edge sites	2.27	$R_{Mn1} = 3.72-3.76$; $R_{Mn2} = 3.20-3.21$	Sun <i>et al.</i> (2018); Sun <i>et al.</i> (2019a)
Aluminum (hydr)oxides	Transition aluminas	XPS	8.6-9.1	Adsorbate intraparticle diffusion followed by sorption	/	/	Papelis (1995)
	Transition aluminas	EXAFS	9.0	6-coordinated mononuclear complexes (at low Γ); formation of a disordered Cd hydroxide or Cd hydroxocarbonate precipitate (at high $[Cd]_i$) ^b).	2.33; 2.35	— $R_{Cd} = 3.84$	Papelis <i>et al.</i> (1995)

	Gibbsite	EXAFS	6	double-corner (bidentate-binuclear) surface complexes	2.12-2.29	R _{Cd} = 3.11-3.16; R _{Al} = 3.29-3.30	Gräfe <i>et al.</i> (2007)
	γ -Al ₂ O ₃	XRD, TEM, EXAFS	7.5	In addition to adsorption complexes and Cd-Al LDH, Cd hydroxide phases were formed at the initial stages of Cd(II) sorption and gradually transformed to CdCO ₃ with time	/	/	Sun <i>et al.</i> (2019b)
Aluminosilicates	Perthitic feldspar, muscovite	XPS, EXAFS	5.4	Only outer-sphere complexes	2.26	/	Farquhar <i>et al.</i> (1997)
	Biotite	XPS, EXAFS	5.4	A combination of inner-sphere complexation and ion exchange mechanisms	/	/	Farquhar <i>et al.</i> (1997)
	Kaolinite	EXAFS	6	dominantly (>75%) outer sphere complexes and a small fraction of CdOHCl complexes	2.24-2.35	R _{Cd} = 3.46-3.73	Gräfe <i>et al.</i> (2007)
	Kaolinite	EXAFS	7.0-9.0	Dominantly outer-sphere adsorption complexes (pH 7); dominantly inner-sphere adsorption complexes on edge sites (pH 9)	2.27; 2.26	— R _{Al/Si} = 3.34	Vasconcelos <i>et al.</i> (2008)

^{a)}Surface loading/coverage, or sorption density; ^{b)}initial Cd concentration; ^{c)}final pH.

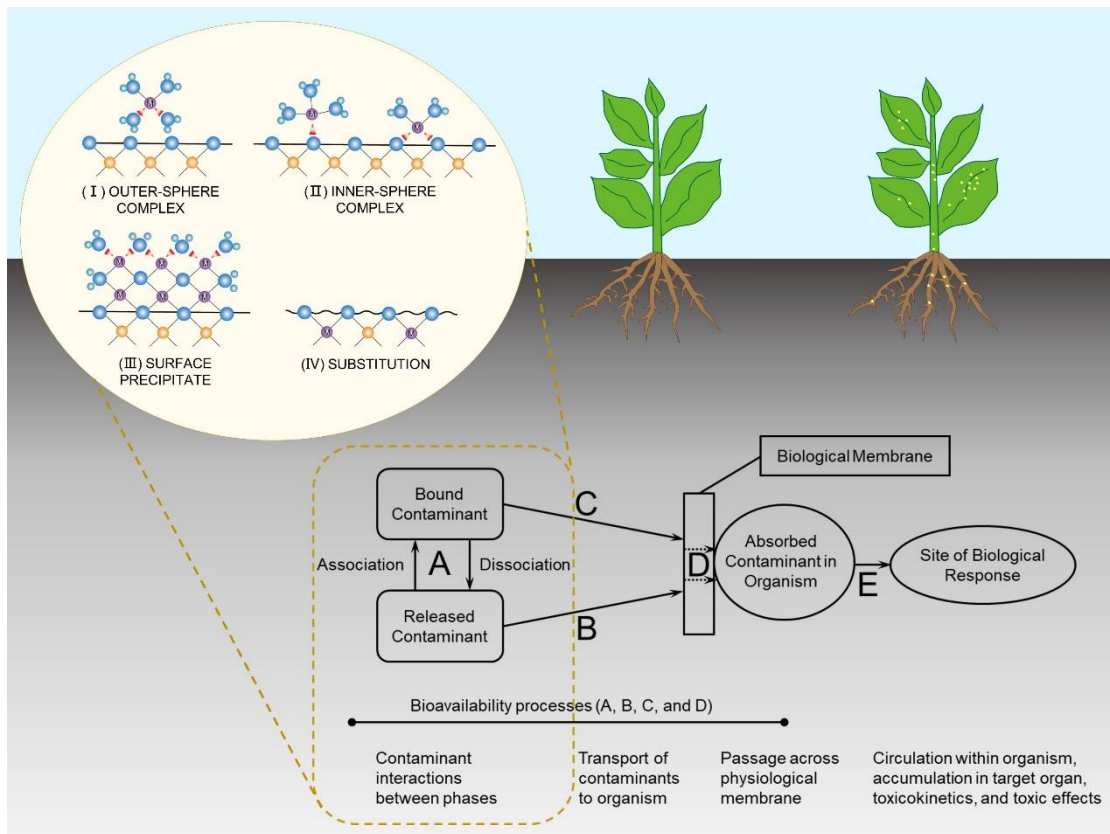


Fig. 1

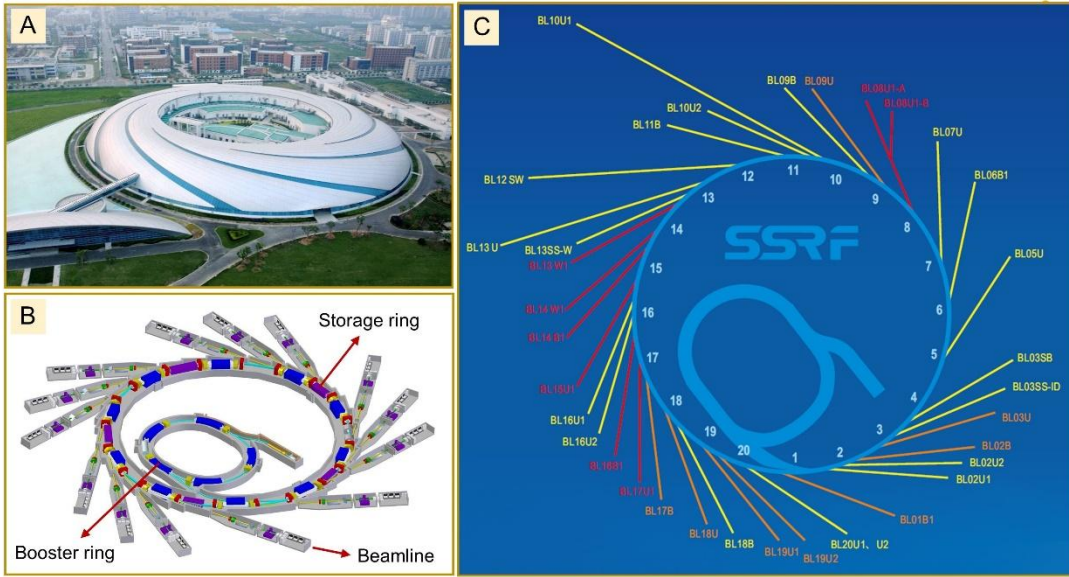


Fig. 2

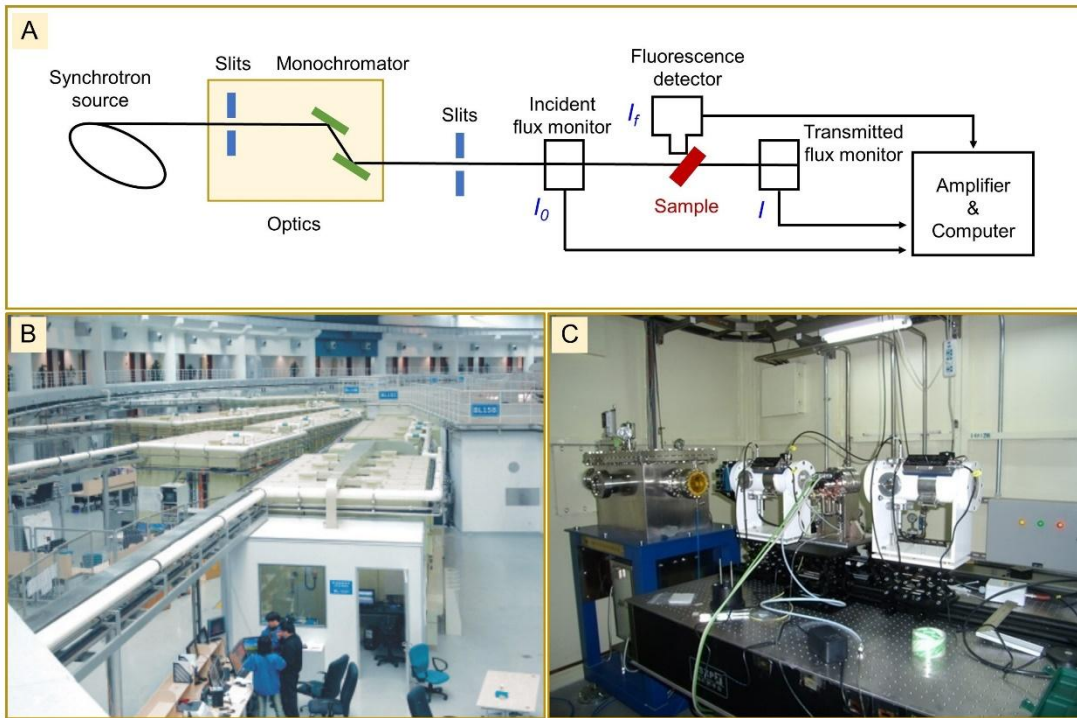


Fig. 3

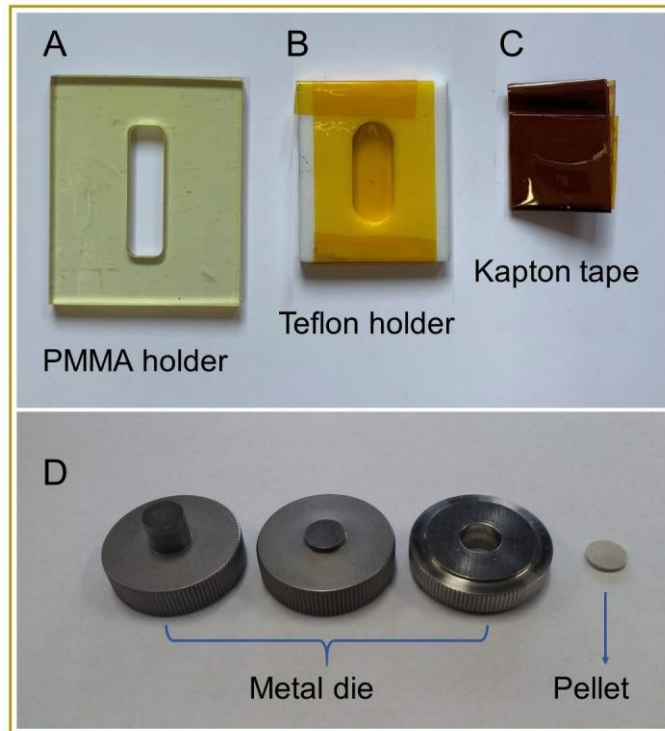


Fig. 4

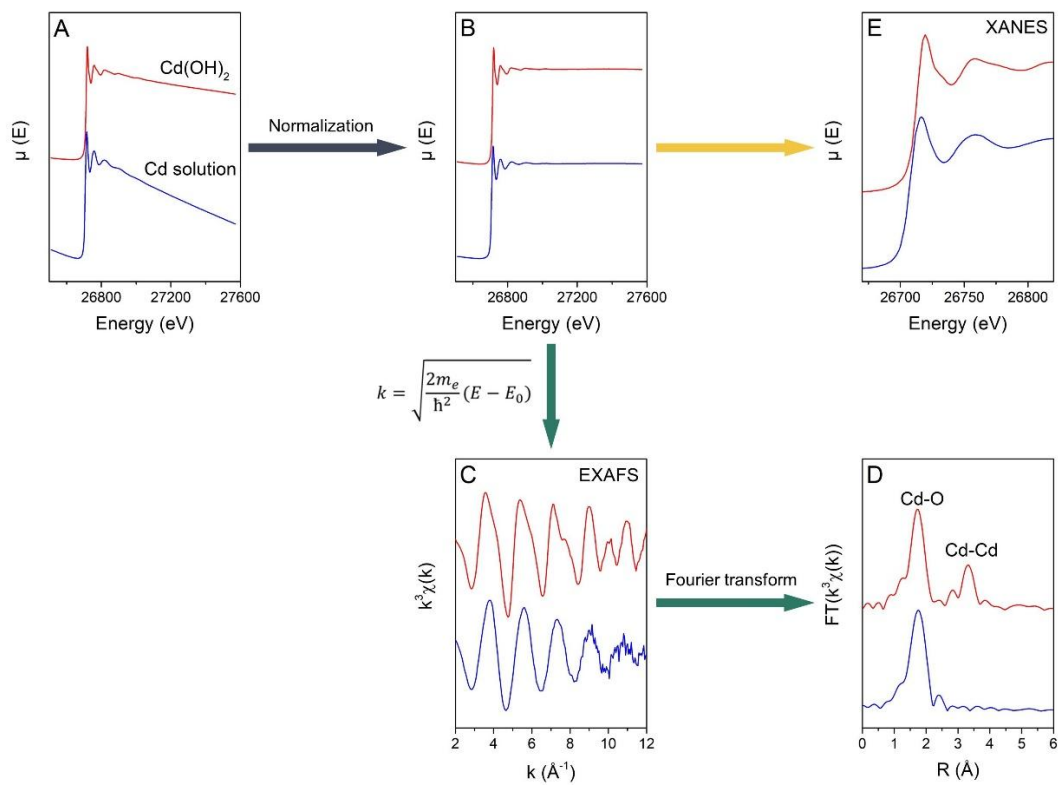


Fig. 5

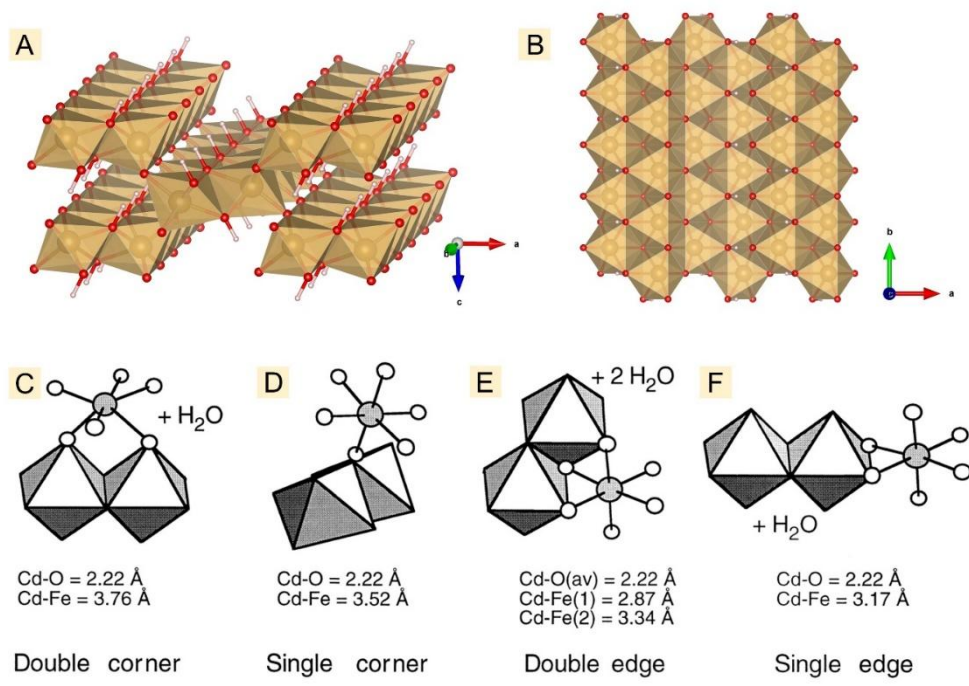


Fig. 6

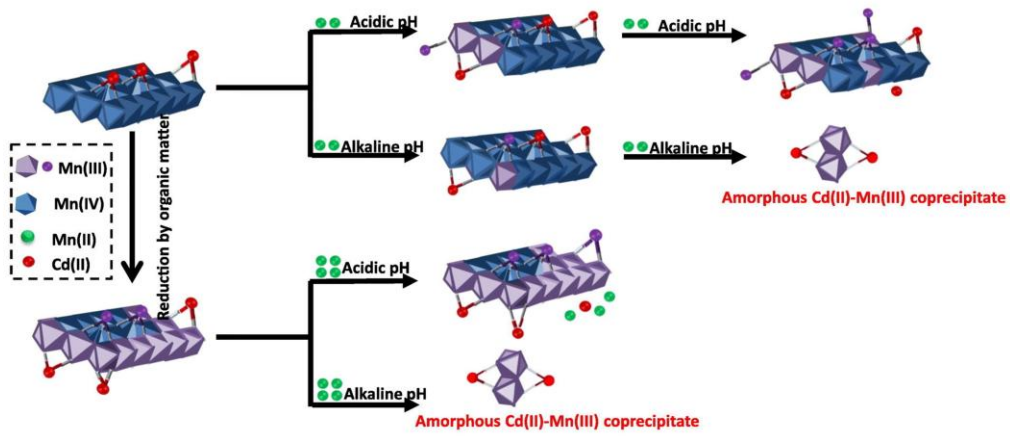


Fig. 7

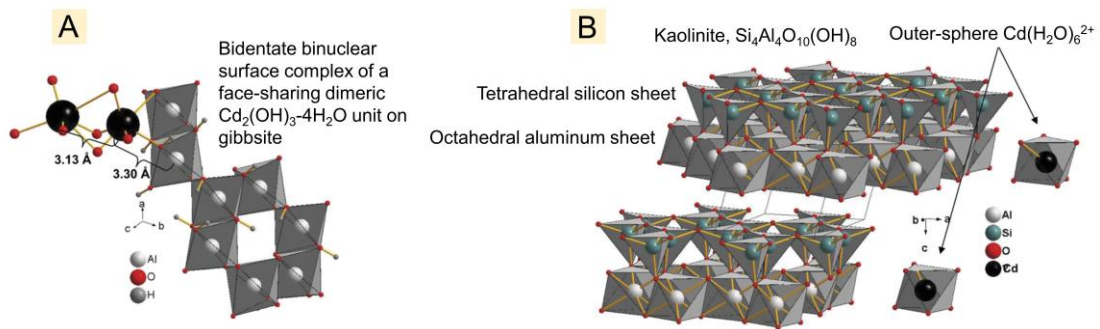


Fig. 8

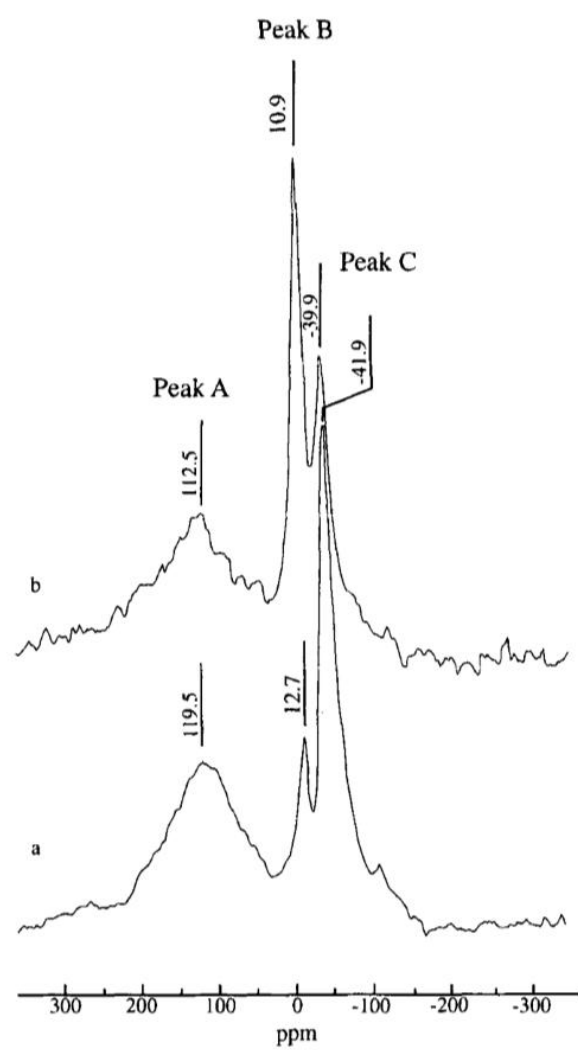
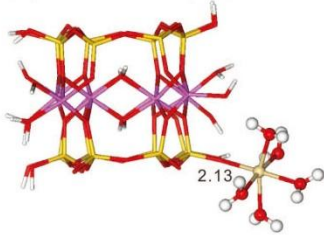
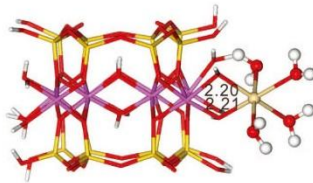


Fig. 9

(A) $\equiv\text{SiO}-\text{Cd}(\text{H}_2\text{O})_5$



(B) $\equiv\text{Al}(\text{OH})_2-\text{Cd}(\text{H}_2\text{O})_4$



(C) Octahedral vacancy

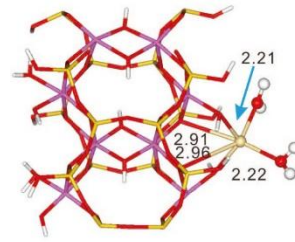


Fig. 10